Anthropological Science
Vol. 132(1), 13–26, 2024

# Identification of functionally related adaptations in the trabecular network of the proximal femur and tibia of a bipedally trained Japanese macaque

Marine Cazenave[1,2,3]*, Masato Nakatsukasa[4], Arnaud Mazurier[5], Matthew M. Skinner[2]

[1]*Division of Anthropology, American Museum of Natural History, New York, NY 10024, USA*
[2]*Skeletal Biology Research Centre, School of Anthropology and Conservation, University of Kent, Canterbury CT2 7NZ, UK*
[3]*Department of Anatomy, Faculty of Health Sciences, University of Pretoria, 0084, Pretoria, South Africa*
[4]*Laboratory of Physical Anthropology, Department of Zoology, Graduate School of Science, Kyoto University, Kyoto, 606-8502 Japan*
[5]*Institut de Chimie des Milieux et Matériaux de Poitiers (IC2MP), Université de Poitiers, UMR CNRS 7285, F-86073 Poitiers, France*

Received 17 July 2022; accepted 14 July 2023

**Abstract** The axial and appendicular skeleton of Japanese macaques (*Macacca fuscata*) trained to adopt bipedal posture and locomotion display a number of functionally related external and internal macro- and micromorphological changes, including site-specific cortical and trabecular bone adaptations. In this study we use high-resolution microtomography scanning to analyse the three-dimensional distribution of the trabecular architecture of the proximal femur and proximal tibia of Sansuke, a male individual trained in bipedal performances for eight years, as well as five wild individuals. The distribution and architecture of trabecular bone in the femoral head of Sansuke is distinct from that found in wild *M. fuscata* individuals, with a unique bone reinforcement around the region of the fovea capitis. Conversely, wild individuals exhibit two pillar-like, high-density structures (converging in an inverted cone) that reach distinct regions of the posterior and anterior surfaces of the femoral head. For Sansuke's proximal tibia, contrary to previous observations from the corticotrabecular complex distribution at the plateau, our results do not show a more asymmetric distribution between medial and lateral condyles with a medial reinforcement. Additionally, relative bone volume in this region is not significantly higher in Sansuke. However, we observed a slightly more medially placed bone reinforcement in the lateral condyle compared with the wild individuals as well as a slightly higher trabecular bone anisotropy in the medial than in the lateral condyle not observed in the wild individuals. These analyses provide new evidence about the nature and extent of functionally related adaptive arrangements of the trabecular network at the coxofemoral and the knee joints in individuals recurrently experiencing atypical load.

**Key words:** bipedally trained *Macaca fuscata*, internal bone structure, functional adaptation

## Introduction

### Background

According to the *saru-mawashi* tradition, juvenile male Japanese macaques (*Macaca fuscata*) are trained to acquire a bipedal posture and, when they can stand stably, are trained to walk for 2–3 km daily (~30–60 minutes in duration) while they spend the remaining time running and climbing similarly to other wild monkeys (Hayama, 1986; Preuschoft et al., 1988). Kinematics, biomechanics, and skeletal morphology in bipedal performing Japanese macaques have been previously investigated, and this forced transition from solely quadrupedal locomotion to the inclusion of bouts of bipedal posture has been regarded as a potentially useful analogue for the evolution of human bipedalism (Hayama et al., 1992; Nakatsukasa, 2004; Hirasaki et al., 2006; Ogihara et al., 2010).

Locomotor kinematics (Hirasaki et al., 2004; Nakajima et al., 2004; Ogihara et al., 2005, 2007, 2018) and energetics (Nakatsukasa, 2004; Nakatsukasa et al., 2006) in *saru-mawashi* monkeys have been studied to assess the unique dynamics associated with bipedal walking, and the neurophysiology of the mechanisms of locomotor control (Mori et al., 2001, 2004, 2006; Nakajima et al., 2004). During bipedal walking an increased load bearing is acting on trunk and hindlimbs and there is a higher instability of the centre of mass. The hip and knee joints of trained macaques are partially flexed, abducted, and laterally rotated (Okada, 1985; Nakajima et al., 2004). Additionally, proximal joint angles measured in the parasagittal plane (e.g. trunk and hip angles) differ between quadrupedal and bipedal gaits, whereas more distal joints (e.g. knee and ankle angles along the parasagittal plane) exhibit smaller differences.

*Correspondence to: Marine Cazenave, Division of Anthropology, American Museum of Natural History, New York, NY 10024, USA.
E-mail: marine.cazenave4@gmail.com

Published online 21 December 2023
in J-STAGE (www.jstage.jst.go.jp) DOI: 10.1537/ase.2307142

For bipedally trained macaques (trained for 2–5 years to walk quadrupedally or bipedally on a motor-driven treadmill), a bipedal gait requires higher but non-uniform electromyographic activity and more coactivation of proximal and distal muscles than during their quadrupedal gait (Higurashi et al., 2018). The duty factor (measured as the stance phase duration on the total step cycle duration) also increases from a quadrupedal to bipedal gait, and the relative duration of the hindlimb double-support phase increases even more (by ~20%). Proportionally longer stance and double-stance phases are consistent with optimal temporal and spatial distribution of increased hindlimb load (Higurashi et al., 2018).

In the hip, during bipedal walking of trained Japanese macaques, important compressive loads are dissipated through the sacroiliac toward the coxofemoral joint, related to the alignment between the gravitational force and the greater length of the ilium (Nakatsukasa et al., 1995). The hip is generally more extended (by ~30°), and its excursion measured on a parasagittal plane is smaller (by ~20°) during a bipedal versus quadrupedal gait (Higurashi et al., 2018). Smaller hip excursion favours stability by limiting the pitch of the upright trunk. In bipedal standing, the femur is abducted and the hip joint flexed. Because of the flexed hip joint, the centre of gravity is located in front of the joint, resulting in a load shift from the caudal to the cranial part of the acetabulum as well as a flexing torque of the trunk about the hip. The abducted femur is balanced by adducting muscles, the m. gluteus medius, whose activity is necessary for the extension of the hip and produces an abducting moment. Major muscles that act against the abducting moment are the adductors, m. gracilis, and hamstrings, as well as the m. biceps femoris, which are all involved in the maintenance of equilibrium (Nakatsukasa et al., 1995).

During bipedal locomotion of trained Japanese macaques, the knee is more extended and laterally rotated on the femur with a valgus position, resulting in more load being directed towards the medial compared with the lateral condyle (Hirasaki et al., 2004; Ogihara et al., 2009; Mazurier et al., 2010). Additionally, more extended knee joints and inverted pendulum-like motion during a bipedal gait creates anterior loading of the tibial plateau (Hirasaki et al., 2004; Mazurier et al., 2010). The knee angle shifts only marginally (<10°) and its excursion in the parasagittal plane remains similar (~70°) during a bipedal gait. However, its cycle-averaged kinematic profile changes with maximal extension occurring just before touchdown, while the knee extension seen before toe-off in a quadrupedal gait is absent during a bipedal gait (Higurashi et al., 2018).

Several morphological and biomechanical studies have investigated the degree to which different skeletal sites adapt to withstand the joint loads and stresses associated with enforced bipedal standing and walking (Nakatsukasa et al., 1995; Nakatsukasa and Hayama, 2003). Functionally related external skeletal changes include the appearance of lumbar lordosis, increased size of the sacroiliac and hip joints, and larger auricular surfaces (Hayama et al., 1992; Preuschoft et al., 1988; Nakatsukasa et al., 1995). In the hindlimb, changes include posteroproximal extension of the femoral head surface, a longer axial diameter of the femoral neck relative to the head–neck length, larger knee-joint surfaces, and retroflexion and accentuated concavity of the tibial medial condyle (review in Nakatsukasa et al., 1995). As a whole, these features reflect the causal relationships between function and adaptation of skeletal morphology (e.g. Skerry, 2000; Pearson and Lieberman, 2004; Ruff et al., 2006).

One of the most well-studied bipedally trained *M. fuscata* is a male specimen called Sansuke. Over a period of eight years he regularly engaged in bipedal performances of 30–60 minutes that resulted in bipedal walking for 2–3 km per day and spent the remaining time running and climbing similarly to other wild monkeys (Nakatsukasa and Hayama, 2003). Given the modelling response of cortical and trabecular bony tissues to site-specific loading environments (Allen and Burr, 2014; Kivell, 2016; Barak, 2020), a number of studies have compared the bone structure of Sansuke to the typical condition of wild Japanese macaques (Macchiarelli et al., 2001; Richmond et al., 2005; Volpato et al., 2008; Mazurier et al., 2010). Based on two-dimensional (2D) planar radiographic imaging of the ilium, Sansuke shows an expanded dorsal bundle and a denser, more anisotropic trabecular network of the iliac body as a whole, as well as a thicker, vertically oriented pillar-like and ventral bundle (Macchiarelli et al., 2001; Volpato et al., 2008). These results have been interpreted as an adaptive response to more compressive loads dissipated through the sacroiliac joint towards the coxofemoral joint, related to the alignment between the gravitational force and the greater length of the ilium (Nakatsukasa et al., 1995; Volpato et al., 2008). Less distinct morphostructural changes have been found in Sansuke's proximal femur (Volpato et al., 2008), with only minor modifications affecting the vertical bundle running from the upper head towards the neck (strengthened in Sansuke) and the area surrounding the trochanteric fossa (extended in Sansuke; Macchiarelli et al., 2001). Finally, a microtomographic investigation of the distal femur found an increase in the degree of trabecular anisotropy in the medial condyle (with a more sagittal orientation), probably reflecting the stereotypical loading that has been observed in Sansuke compared to the wild macaque condition (Richmond et al., 2005).

Such evidence from the distal femur is also supported by a microtomographic study of the proximal tibia, which revealed an absolutely and relatively thicker corticotrabecular complex in Sansuke's articular plateau (Mazurier et al., 2010). Indeed, while the corticotrabecular complex of the medial plateau of the proximal tibia is thicker than the lateral one in both Sansuke and wild macaques, the topographic contrast in the trained individual is much greater, with marked thickening measured at the level of the anterior portion of the articular surface (Mazurier et al., 2010). Also, Sansuke's lateral tibial condyle shows a relatively more homogeneous corticotrabecular distribution and a slight anteroposterior thinning of the cortex. This indicates greater loads acting on the medial condyle, probably resulting from more laterally rotated hip and knee joints (Hirasaki et al., 2004, Ogihara et al., 2009). Biomechanically, an anterior reinforcement of the tibial plateau probably plays an important role in the absorption and

dissipation of loads related to more extended hip and knee joints and the use of inverted pendulum-like gait mechanics during bipedal locomotion (Hirasaki et al., 2004). In this study, we expand on previous analyses of Sansuke's skeleton with a whole-epiphysis microtomographic analysis of the femoral head and proximal tibia.

Based on an increasing number of studies demonstrating trabecular bone modelling in response to biomechanical loading during an individual's lifetime (e.g. Tsegai et al., 2013, 2018; Cazenave et al., 2017, 2019, 2021; Su and Carlson, 2017; Georgiou et al., 2018, 2019, 2020; Dunmore et al., 2019; 2020a, 2020b; Sukhdeo et al., 2020; Bird et al., 2021, 2022; see Kivell, 2016 and references therein), the last two decades have seen several important conceptual and technological advances in the high-resolution three-dimensional (3D) imaging, quantification, and statistical comparison of the internal bone structural variation (e.g. Pahr and Zysset, 2009; Bondioli et al., 2010; Puymerail, 2013; Sylvester and Terhune, 2017; DeMars et al., 2021; Profico et al., 2021; Veneziano et al., 2021; Bachmann et al., 2022). However, "the confidence with which internal bone structures can be used to retrodict behaviour in fossil species remains a work in progress" (Almécija et al., 2021). Therefore, quantitative analyses of the internal bone structure of joints in individuals of known behaviour can enhance our understanding of the links between trabecular modelling and mechanical function, and allow stronger inferences on the behaviour of fossil taxa (Biewener et al., 1996; Guldberg et al., 1997; Robling et al., 2002; Mittra et al., 2005; Pontzer et al., 2006; Ruff et al., 2006; Polk et al., 2008; Barak et al., 2011; Harrison et al., 2011; Christen et al., 2014). In this respect, the case of bipedally trained Japanese macaques, such as Sansuke, is of particular value. By using X-ray microCT and cutting-edge 3D imaging techniques, we extend previous studies on Sansuke's endostructural bony adaptations (Macchiarelli et al., 2001; Richmond et al., 2005; Volpato et al., 2008; Mazurier et al., 2010) by comparatively assessing its trabecular architecture in the proximal femur and proximal tibia.

### Predictions

Based on the evidence of a higher and more compressive load vertically oriented in the caudal region of the acetabulum during bipedal posture and gait in trained macaques, and on the assumption that the trabecular bone of the femoral head is sensitive enough to model according to the loading conditions during the bipedal posture and locomotion in Sansuke (which only represent a short amount of time in his daily life) as seen in the pelvic bone (Volpato et al., 2008), we predict finding in Sansuke's femoral head a pattern of trabecular architecture distinct from that found in wild *M. fuscata*. Specifically, we expect this to be characterized by an approximately superoinferiorly oriented bone reinforcement resulting from more vertical loading at the proximal femoral head during bipedal locomotion. This will be associated with higher relative bone volume, thicker trabeculae, and a higher degree of anisotropy in Sansuke (Nakatsukasa et al., 1995, Volpato et al., 2008).

Based on the evidence of a more pronounced medial loading in the tibial articular surface compared with the lateral plateau resulting from the more laterally rotated tibia on the femur (Hirasaki et al., 2004, Ogihara et al., 2009), as well as anterior loading related to a more extended hindlimb joint and the use of an inverted pendulum-like motion during bipedal locomotion (Hirasaki et al., 2004), compared to the typical condition of wild individuals, in Sansuke we expect to find: (i) a more asymmetric distribution in relative bone volume between the medial and the lateral condyles that is associated with an increase in the anterior region of the medial condyle; and (ii) greater bone volume fraction associated with a higher degree of anisotropy. This expectation is based on the assumption that the trabecular bone of the proximal tibia is sensitive enough to model according to the loading conditions during the bipedal posture and locomotion in Sansuke as seen in the corticotrabecular complex of the tibial plateau (Mazurier et al., 2010).

## Materials and Methods

We investigated the left and right proximal femora and tibiae of Sansuke, a 10-kg male *M. fuscata* engaged in bipedal performances lasting 30–60 minutes/day (Hayama, 1986; Preuschoft et al., 1988) from the age of 2 years until his death at the age of 10 years (Nakatsukasa and Hayama, 2003). The comparative sample consists of five right proximal femora (from four likely male and one likely female individuals, based on skeletal size) and five right proximal tibiae (all likely male, based on skeletal size) from non-bipedally trained wild individuals of the same taxon. Four of the five femora and tibiae are associated. All specimens lack macroscopic evidence of alteration or pathological changes, and are housed at the Laboratory of Physical Anthropology, Kyoto University (Japan). Details on the composition of the sample are provided in Supplementary Table S1.

Sansuke's femora and tibiae and one femur and two tibiae from wild individuals were scanned in 2005 by synchrotron radiation microtomography (SR-μCT) at the European Synchrotron Radiation Facility (ESRF) medical beam line ID17, Grenoble (details in Mazurier et al., 2010). The voxel size of the reconstructed volume is $45.5 \times 45.5 \times 43.6\ \mu m^3$. The remaining samples (four femora and three tibiae) were scanned in 2022 at the Laboratory of Physical Anthropology, Kyoto University, using a ScanXmate A080s (Comscan Co.) with an isotropic voxel size of 41.9 μm, for the proximal femora, and ranging from 54.6 μm to 59.0 μm, for the proximal tibiae (Supplementary Table S1).

All specimens were virtually reoriented in Avizo v. 9.0 software (Visualization Sciences Group Inc., Bordeaux) using a landmarking-based automatic alignment. The proximal femora were then virtually cut at the head–neck junction, and the tibia were cut at the level of the tuberosity perpendicular to the main axis of the proximal portion of the shaft.

All oriented bones were segmented using MIA-Clustering segmentation (Dunmore et al., 2018) to automatically isolate bone from air and then processed with Medtool 4.6 (http://www.dr-pahr.at). In Medtool 4.6, we followed the procedure detailed in Gross et al. (2014) and

Tsegai et al. (2018). First, the whole bone was segmented by a 'fill' operation that casts rays from the outer cortical shell at multiple angles followed by a morphological closing step. A series of morphological filters were then applied to identify and remove the cortical shell, thus isolating the trabecular structure. A 3D background grid with node spacing of 2.5 mm was superimposed on the isolated trabecular volume, and overlapping spherical volumes of interest (VOI), 5 mm in diameter, were centred at each of its nodes. Trabecular bone volume fraction (BV/TV), trabecular thickness (Tb.Th.), trabecular spacing (Tb.Sp.), and degree of anisotropy (DA) were measured in each VOI and the values interpolated on the centroids of a 3D tetrahedral mesh of the trabecular volume created with the Computational Geometry Algorithms Library. Morphometric maps of the distribution of each parameter can then be visualized (additional technical details in Tsegai et al., 2018).

Statistical analyses were performed in RStudio v. 1.2.5033 running with R v. 3.4.4 (R Core Team, 2018). Plots were generated using ggplot2 (Wickham, 2009). Standardized measures were calculated for interspecific comparisons, in which for each individual the raw values of each parameter were divided by the individual mean of all values of this parameter. For each standardized parameter, the significance of the two-by-two individual differences was tested by the non-parametric pairwise Wilcoxon rank sum tests with a Bonferroni correction as well as two-sample *t*-test via Monte Carlo sampling with 1000 permutations. Given that for each specimen a set of hundreds of VOIs is extracted sampling the whole bone, with four variables measured in each VOI, pairwise Pearson correlation tests between the four variables have been conducted for each specimen. These tests aim to measure, for each specimen, the degree of correlation between the distributions throughout the bone of the investigated parameters. Following Chan (2003), $r > 0.8$ shows a high correlation, $0.6 < r < 0.8$ shows a moderate correlation and $r < 0.6$ shows a poor correlation. A significance threshold of 0.05 for the *P*-values was adopted for all statistical analyses.

## Results

### Proximal femur

Figure 1 presents morphometric maps in medial view of the distribution of the four investigated trabecular parameters (BV/TV, Tb.Th., Tb.Sp., and DA) in Sansuke's left and right femoral heads in comparison to those from a wild macaque. The maps of the remaining wild individuals are shown in the online Supplementary Figure S1 and the same results in superior view for all individuals are presented in Supplementary Figure S2. As predicted, in Sansuke there is a distinct pattern of bone distribution from that found in the wild *M. fuscata* individuals. However, the expectation of an approximately superoinferiorly oriented bone reinforcement is not detected. Indeed, in both Sansuke's femoral heads, the BV/TV distribution indicates a reinforcement that is limited to the region of the fovea capitis. Conversely, in KAS 266 and KAS 276 (Figure 1, Supplementary Figure S1, Supplementary Figure S2) two concentrations of relatively higher BV/TV values forming two converging pillar-like structures are found in the posterior and anterior surfaces of the head, respectively. In the other three individuals (KAS 269, KAS281 and KAS 284; Supplementary Figure S1, Supplementary S2), such structures appear as less discrete units, with a continuous concentration of bone density spanning in the superior aspect of the femoral head.

In Sansuke, Tb.Th. distribution matches the BV/TV arrangement, with a concentration of high Tb.Th. values in the region of the fovea capitis, while in the wild individuals a high concentration of Tb.Th. tends to be observed in the posterosuperior surface. However, in this case, for the wild specimens, there is no concentration of high Tb.Th. at the level of the anterior BV/TV pillar-like structure, and the posterosuperior concentration of high Tb.Th. does not extend internally but is confined to the subchondral layers (except for KAS 276, which shows a thin extension of high Tb.Th. toward the neck in the posterior region of the head). In both Sansuke and the comparative sample, Tb.Sp. tends to show lower values on the inferoanterior aspect of the head, while the highest values of DA tend to be found in the head–neck junction, even though the signal in *Sansuke* is less evident. In some wild individuals, an extension of the distribution of the highest DA values in the anterior and posterior surfaces is observed.

Our prediction of overall higher bone density and thicker struts in Sansuke is not supported by our findings. In Sansuke's right femoral head, pairwise Wilcoxon tests show that both variables differ statistically from those measured in three wild individuals (KAS 266, KAS 281, KAS 284) for BV/TV and one wild individual (KAS 266) for Tb.Th. (Figure 2, Supplementary Table S2). However, in Sansuke's left femoral head, no appreciable differences with the wild sample have been found for BV/TV and Tb.Th. In addition, the Monte Carlo permutation tests show no differences for all parameters and all pairwise comparisons. Figure 2 illustrates that the medians of both Sansuke's femoral head BV/TV and Tb.Th. are slightly lower than of the wild sample. It is nonetheless interesting to note that in this trained individual we observe the highest absolute BV/TV and relative BV/TV and Tb.Th. values in individual VOIs of the entire sample (Figure 1, Figure 2). These high values are from the VOIs extracted at the region of the fovea capitis. No appreciable differences have been found for DA and Tb.Sp. (Figure 2, Supplementary Table S2).

The distribution patterns of trabecular parameters shown by the morphometric maps are supported by the correlation tests presented in Table 1. In both Sansuke's femora and in the wild male KAS 269, BV/TV and Tb.Th. are highly correlated ($r > 0.8$; Chan, 2003), which is not the case in the other comparative specimens that show a moderate correlation ($0.6 < r < 0.8$). In Sansuke, a functionally related bone reinforcement at the region of the fovea capitis seems to be achieved through thickening the trabecular struts. Additionally, in Sansuke DA is moderately correlated with BV/TV and it is highly and moderately correlated with Tb.Th. for the left and right femora, respectively. All other tests show poor correlation ($r < 0.6$). All Pearson correlation coefficients are statistically significant ($P \leq 0.05$) except for coefficients $\leq 0.1$ for which interpretation of the results cannot be certain.

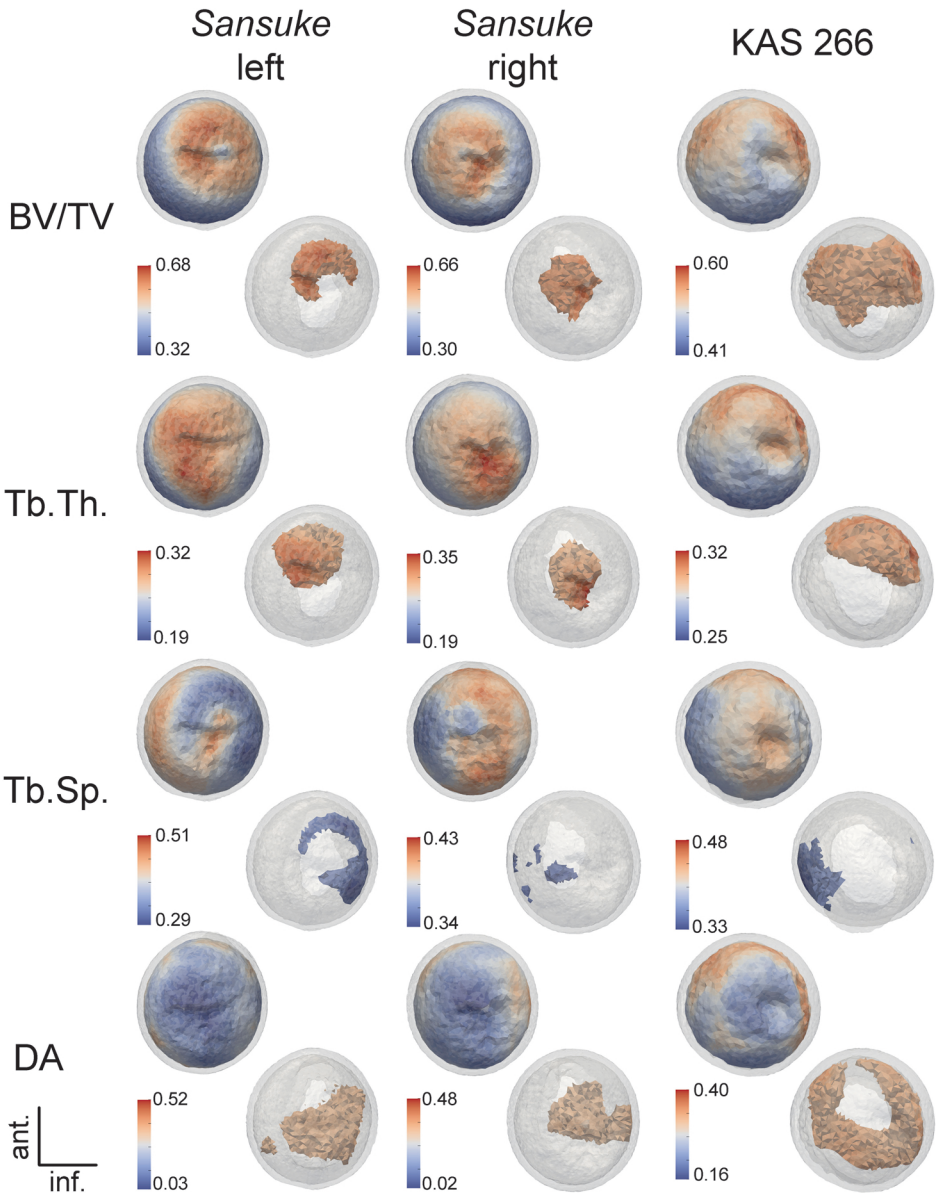


Figure 1. The upper rows represent the virtual morphometric maps, in medial view, of all trabecular bone volume (BV/TV, %), trabecular thickness (Tb.Th., mm), degree of anisotropy (DA), and trabecular spacing (Tb.Sp., mm) values in the femoral heads (only the subchondral layer is therefore visible) of the bipedally trained macaque Sansuke and in the right femur of a wild *Macaca fuscata* (KAS 266). The lower rows represent the deeper portion of the femoral head of the values >80% of the range of variation for the BV/TV, Tb.Th, and DA, and the values <20% of the range of variation for the Tb.Sp. For each individual, chromatic scale ranges from the minimum value (blue) to the maximum value (red). The left femur of Sansuke has been mirrored as a right femur.

**Proximal tibia**

The distribution maps of the four trabecular parameters assessed in Sansuke's left and right proximal tibiae are presented in Figure 3 and compared to those from a wild macaque (note that maps of the other four wild individuals are shown in Supplementary Figure S3). In this case, the results do not follow our first prediction. In Sansuke, the BV/TV distribution does not show a clear asymmetry between medial and lateral condyles, or an anterior structural reinforcement across the whole plate. Indeed, a similar pattern of BV/TV, Tb.Sp., and DA distribution is found in all individuals. Specifically, all investigated proximal tibiae show: (i) a concentration of high BV/TV in the medial area of the medial condyle and in the central area of the lateral condyle (even though the bone reinforcement in the lateral condyle is slightly more medially placed in Sansuke, notably in the left tibia, than in the wild individuals); (ii) the lowest Tb.Sp. values in the posterior area of the articular surface; and (iii) a concentration of high DA values in the central region of the posterior portion. However, the medial condyle tends to be more anisotropic (i.e. higher DA) than the lateral condyle in Sansuke, while no asymmetric distribution of DA is observed in the wild individuals. Moreover, no clear trend can be identified for Tb.Th. distribution apart from highest Tb.Th. values observed in the central intercondylar area and the posterior surface of the proximal dia-

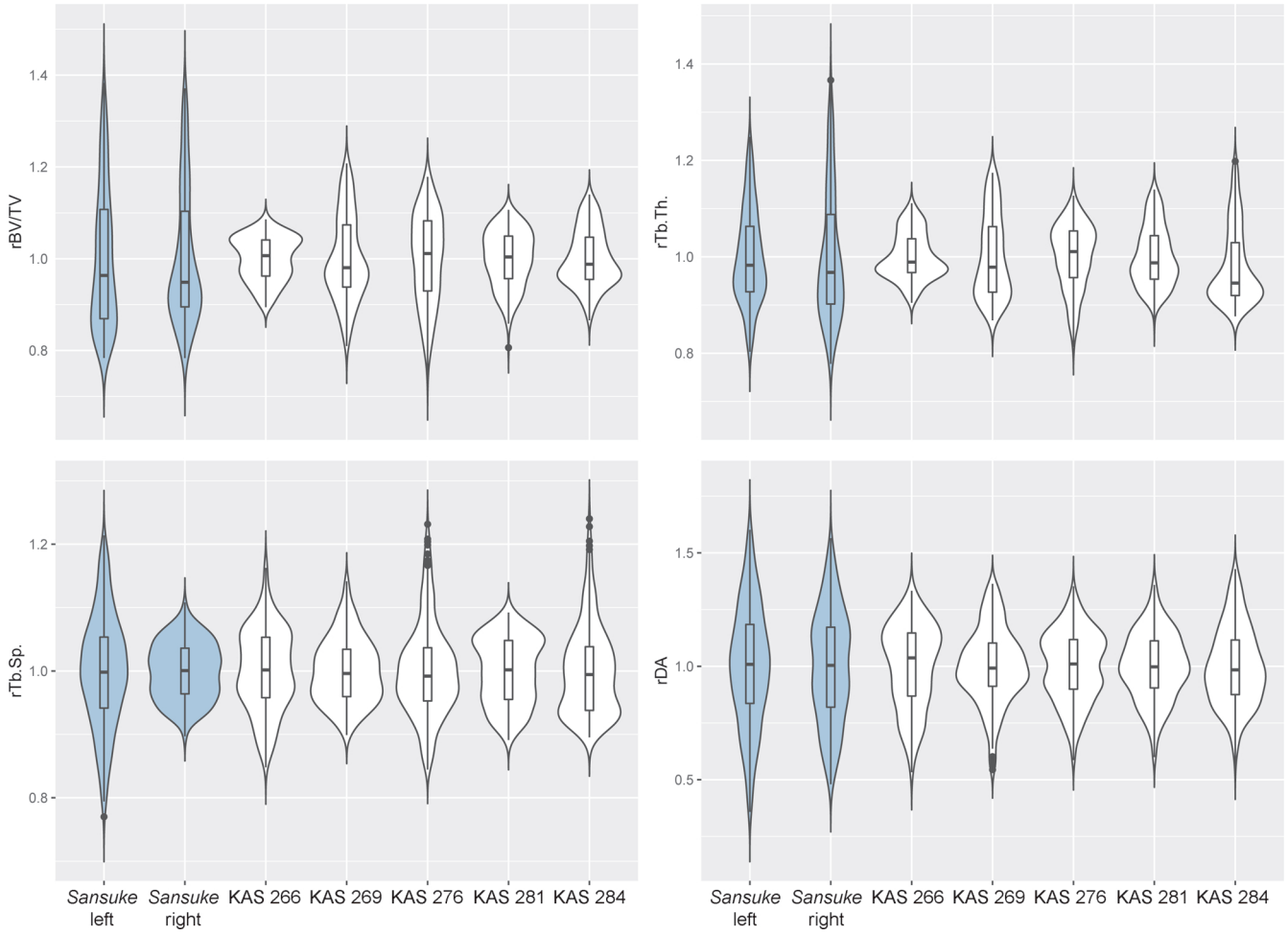


Figure 2. Box and violin plots of relative bone volume (BV/TV), trabecular thickness (Tb.Th.), trabecular spacing (Tb.Sp.), and degree of anisotropy (DA) of the femoral head of the study sample. Values are standardized by the mean for each individual. Violin plots show the kernel density distribution (including the minimum and maximum values) while the box and whisker plots show the median and quartiles.

physis in Sansuke, KAS 276, and KAS 309. Contrary to our second prediction, bone volume fraction and degree of anisotropy are not significantly higher in Sansuke than in the wild *M. fuscata* individuals (Figure 4, Supplementary Table S3). The permutation Monte Carlo tests show no differences for all parameters and all pairwise comparisons.

These qualitative observations are confirmed by the correlation tests presented in Table 2. In all individuals, BV/TV is highly negatively correlated with Tb.Sp. ($r > 0.8$) except for KAS 269, which shows a moderate correlation ($0.6 < r < 0.8$) between the two parameters. BV/TV is highly correlated with Tb.Th. in the right femur of Sansuke and KAS 269, and moderately correlated with Tb.Th. in Sansuke's left femur and all wild individuals, except KAS 276, which shows a poor correlation ($r < 0.6$). Finally, in Sansuke, but not in all wild individuals, Tb.Th. is negatively moderately or highly correlated with DA. All other tests show poor correlations. All Pearson correlation coefficients are statistically significant ($P \leq 0.05$), except for coefficients ≤0.1. Differences in voxel size between the scans might affect the strength of correlations between Sansuke and the comparative sample.

## Discussion and Conclusions

An increasing number of studies have tested the degree to which variation in trabecular bone structure at different skeletal sites reflects differences in locomotor-related loadings in humans and other primates (review in Kivell, 2016). For instance, although the link between the endostructural architecture of the proximal femur and load transfer and dissipation is more complex than assumed by the first mechanical models (e.g. Fajardo et al., 2007; Ryan and Walker, 2010; Shaw and Ryan, 2012), trabecular bone variation in the primate femoral head has provided clear evidence for structural differences across locomotor groups (Fajardo and Müller, 2001; MacLatchy and Müller, 2002; Ryan and Ketcham, 2002a, 2002b, 2005; Ryan and Krovitz, 2006; Saparin et al., 2011; Ryan and Shaw, 2012, 2015; Raichlen et al., 2015; Ryan et al., 2018; Tsegai et al., 2018; Georgiou et al., 2019; Cazenave et al., 2021).

In 2019, a study of trabecular bone structural distribution patterns of the extant great ape femoral head, using a whole epiphysis approach similar to that of the present study, first revealed that holistic evaluations of the trabecular architec-

Table 1. Results of Pearson correlation tests between the trabecular bone density (BV/TV), trabecular thickness (Tb.Th.), trabecular spacing (Tb.Sp.), and degree of anisotropy (DA) of the femoral head calculated for the left and right proximal femora of the bipedally trained macaque Sansuke and for the right femora of five wild *Macaca fuscata*.

| Specimens | Parameters | BV/TV | Tb.Th. | Tb.Sp. |
|---|---|---|---|---|
| Sansuke left | Tb.Th. | **0.96*** | — | — |
| | Tb.Sp. | –0.13* | 0.10 | — |
| | DA | –0.76* | **–0.83*** | –0.04 |
| Sansuke right | Tb.Th. | **0.90*** | — | — |
| | Tb.Sp. | –0.58* | –0.26* | — |
| | DA | –0.77* | –0.71* | 0.35* |
| KAS 266 | Tb.Th. | 0.63* | — | — |
| | Tb.Sp. | –0.38* | 0.45* | — |
| | DA | 0.54* | 0.35* | –0.34* |
| KAS 269 | Tb.Th. | **0.88*** | — | — |
| | Tb.Sp. | –0.44* | 0.00 | — |
| | DA | 0.04 | –0.19* | –0.58* |
| KAS 276 | Tb.Th. | 0.61* | — | — |
| | Tb.Sp. | –0.44* | 0.36* | — |
| | DA | –0.32* | –0.21* | –0.07 |
| KAS 281 | Tb.Th. | 0.76* | — | — |
| | Tb.Sp. | –0.30* | 0.37* | — |
| | DA | 0.10 | –0.14* | –0.47* |
| KAS 284 | Tb.Th. | 0.76* | — | — |
| | Tb.Sp. | –0.10 | 0.45* | — |
| | DA | –0.09 | –0.45* | –0.49* |

Strong correlations ($r > 0.8$) are in bold. *Significant correlations ($P < 0.05$).

ture show patterns linked to locomotor behaviour (Georgiou et al., 2019). More precisely, *Pan* and *Gorilla* demonstrated two concentrations of higher bone density—one in the posterosuperior aspect and one in the anterior portion of the femoral head—consistent with hip orientation and joint loading during two main locomotor modes: knuckle-walking and climbing. These two pillar-like structures extend and converge internally. In *Pongo*, these structures are less evident as discrete units with bone density concentrated as a band across the superior aspect of the femoral head and interpreted as reflecting less discrete and more homogeenous loading of the hip joint during arboreal locomotion (Georgiou et al., 2019, 2020). In terms of general bone density of the femoral head, the five wild *M. fuscata* individuals represented in our study show an ape-like trabecular conformation, but with some variation. Indeed, two specimens show two very distinct pillars, while the other three femora display less discrete pillar-like structures arising from the superior head surface but merged within a topographically nearly homogeneous network. Such endostructural arrangement is consistent with the postural and locomotor modes typical of wild Japanese macaques, which are quadrupeds terrestrially, but also arboreal, with vertical climbing and short-distance leaping (Negayama, 1983; Kimura, 1985; Okada, 1985; Nakano, 1996; Nakano et al., 1996; Chatani, 2003; Fleagle, 2013). They have developed hamstring muscles which function to extend hip joints to propel the body forward (Haxton, 1947; Kimura et al., 1979). Similar to the condition displayed by *Pan* and *Gorilla*, in *M. fuscata* the hip is flexed during the swing phase of quadrupedalism, with a maximum flexion angle of −45° and a mobile (excursion) range of the hip joint of about −65° during a single step cycle (Nakajima et al., 2004). This is consistent with high loading of the posterosuperior region of the femoral head and the relatively higher bone density found in this region. During the resting posture, vertical climbing, and leaping, the hip is highly flexed (Hirasaki et al., 1993; Isler, 2005), which would result in the anterior aspect of the head contacting the lunate surface of the acetabulum. In the wild specimens examined in our study, while the posterosuperior subchondral bone reinforcement is accompanied by thicker struts, this is not the case for an anterior reinforcement. As a whole, these results indicate that additional investigations are needed for a better understanding of the functional significance of the intra-individual topographic variation of the femoral head trabecular network in extant primates displaying different locomotor modes, and especially of the direct links between hypothesized load environment and site-specific microstructural arrangement. A future area of investigation would be finite-element analyses, and in particular inverse-bone remodelling (Synek et al., 2019) and homogenized finite elements (Bachmann et al., 2022) that are sensitive enough to detect differences in external joint loadings in primates from bone microarchitectures.

In agreement with our first two predictions, Sansuke's femoral head does show a global pattern of bone density and trabecular thickness distribution distinct from the wild macaque condition. However, contrary to our expectation based on a previous analysis of the iliac textural characteristics (Volpato et al., 2008), Sansuke does not show a developed superoinferior bone reinforcement resulting from more vertical loading at the proximal femoral head occurring during bipedal performances, and overall BV/TV and Tb.Th. values do not discriminate Sansuke from the wild macaques. Given that, like wild macaques, Sansuke's main activities were running and climbing, this result questioned whether the trabecular bone of the femoral head was sensitive enough to model according to the loading conditions encountered during bipedal activities, and suggests that the trabecular bone architecture of the femoral head does not only reflect the less stereotyped and multiaxial loading conditions of a wild-like locomotor behaviour. Nonetheless, a concentration of high bone density along with thick struts is uniquely found in Sansuke in the region of the fovea capitis, and this non-articular depression provides attachment to the ligamentum teres.

In humans, the ligamentum teres mainly carries out a stabilizing function of the hip joint (Rao et al., 2001; Philippon et al., 2014; O'Donnell and Arora, 2018), but also limits hip adduction during a bipedal gait (Kaplan, 1949; Delcamp et al., 1988; Gray and Villar, 1997; Rao et al., 2001; Demange et al., 2007; Kapandji, 2011; Guanche, 2012; van Arkel et al., 2015; O'Donnell et al., 2018). In Sansuke, rather than a pillar-like structure superoinferiorly crossing the femoral head, a bone reinforcement in the re-

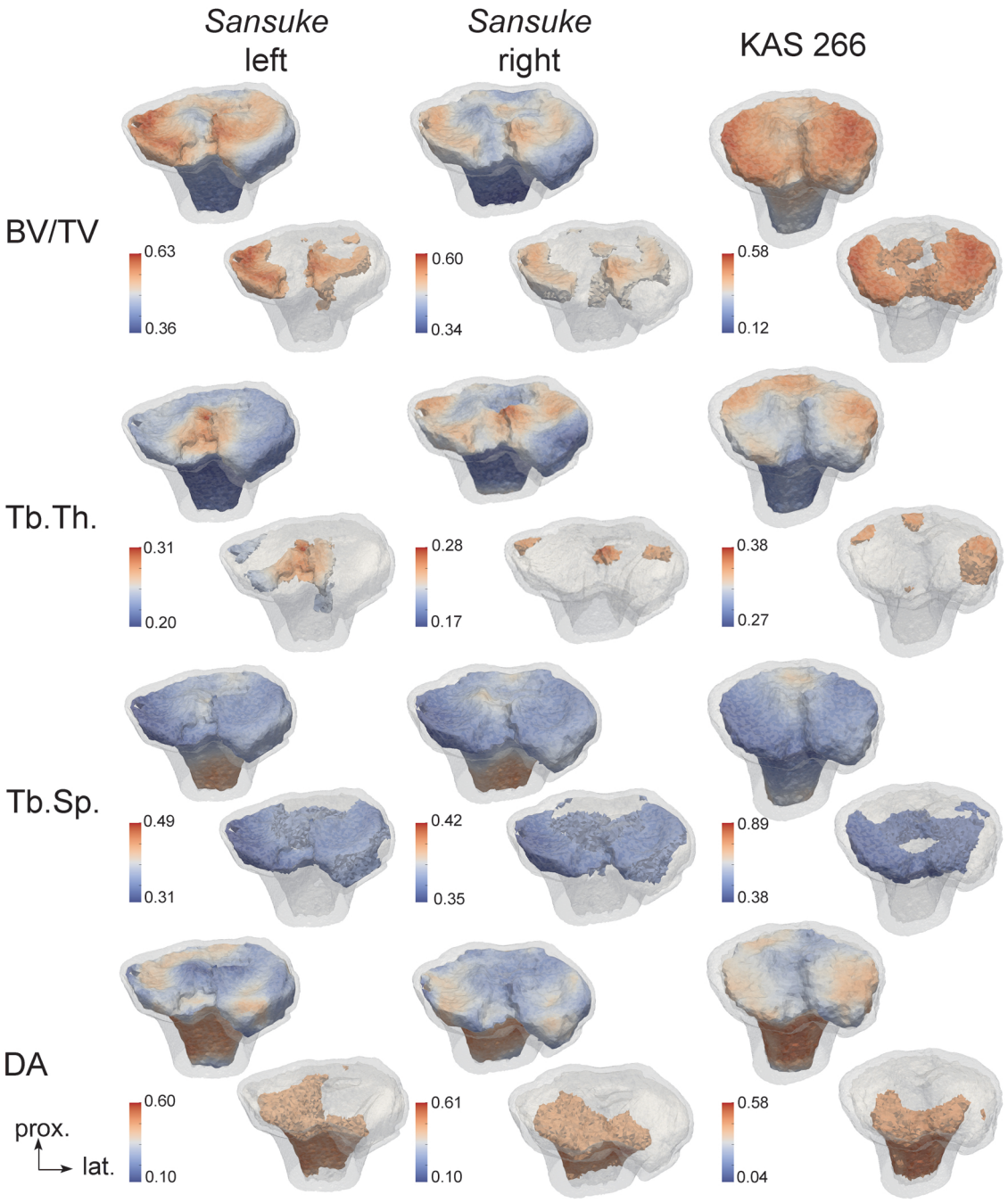


Figure 3. The upper rows represent the virtual morphometric maps, in medial view, of all trabecular bone volume (BV/TV, %), trabecular thickness (Tb.Th., mm), degree of anisotropy (DA), and trabecular spacing (Tb.Sp., mm) values in the proximal tibiae (only the subchondral layer is therefore visible) of the bipedally trained macaque Sansuke and in the right proximal tibia of a wild *Macaca fuscata* (KAS 266). The lower rows represent the deeper portion of the proximal tibia of the values >80% of the range of variation for the BV/TV, Tb.Th, and DA, and the values <20% of the range of variation for the Tb.Sp. For each individual, chromatic scale ranges from the minimum value (blue) to the maximum value (red). The left tibia of Sansuke has been mirrored as a right tibia.

gion of the insertion of the fovea capitis might represent the functionally related structural response to the need to stabilize the hip joint during the bipedal-like trained cycle in relation to the recurrent instances of adduction (Nakatsukasa et al., 1995; Ogihara et al., 2009, 2018), and is associated with the posteroproximal extension of his femoral head surface (Nakatsukasa et al., 1995).

While locomotor-related variation of the proximal femur inner architecture has received considerable attention, research into the endostructural signal of the proximal tibia has focused on human clinical studies (Ritter et al., 2014; Burnett, 2017; Roberts et al., 2017; Renault et al., 2020; Goliath et al., 2022) and remains poorly investigated in non-human extant primates and fossil hominins (Ahluwalia, 2000; Mazurier et al., 2010).

Comparative functional anatomy shows that the mam-

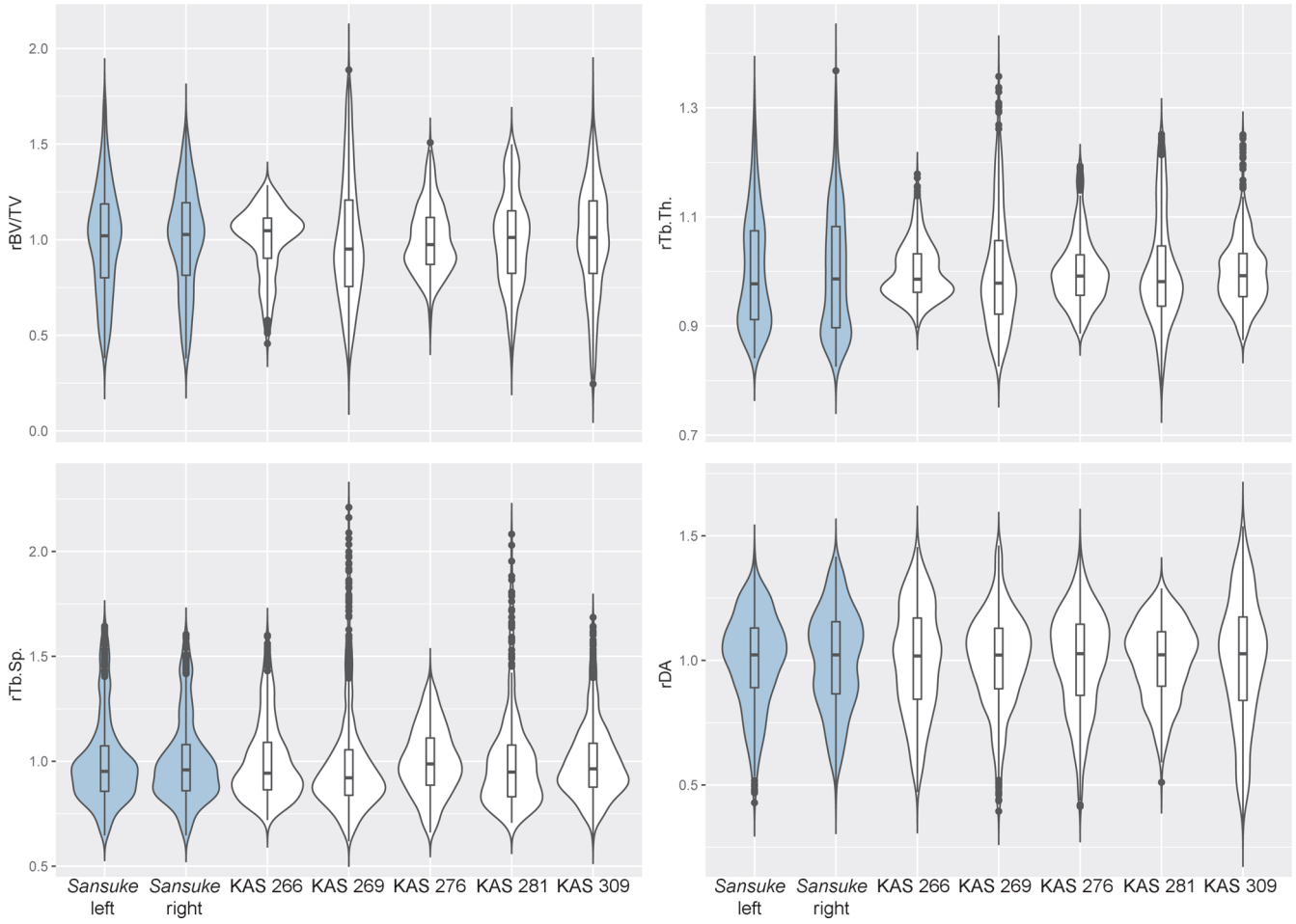


Figure 4. Box and violin plots of relative bone volume (BV/TV), trabecular thickness (Tb.Th.), trabecular spacing (Tb.Sp.), and degree of anisotropy (DA) of the proximal tibia of the study sample. Values are standardized by the mean for each individual. Violin plots show the kernel density distribution (including the minimum and maximum values) while the box and whisker plots show the median and quartiles.

malian knee is "an alarmingly complex joint" (Lovejoy, 2007). In the primate proximal tibia, variation exists in the size and shape of the medial and lateral articular surfaces and the proportions of the intercondylar tubercles of the plateau (Tardieu, 1983; Lovejoy, 2007), reflecting adaptations to a wide range of postural and locomotor modes (Aiello and Dean, 1990). Accordingly, comparative and experimental investigations on the endostructural arrangement of the proximal tibia in extant primate taxa have the potential to provide a valuable framework for interpreting the internal bone condition from fossil hominin specimens (Mazurier et al., 2010).

In Sansuke, none of the expectations based on the evidence of a thicker corticotrabecular complex heterogeneously distributed beneath the articular surface of the proximal tibia (Mazurier et al., 2010) are supported by our analyses. Sansuke does not show an average higher bone density compared with the wild macaques, nor the highest bone density values. Additionally, we could not identify a greater degree of asymmetry in trabecular bone volume distribution between the two condyles compared with the wild individuals, and no trabecular variables are distinct. However, in Sansuke's tibia there is a slightly more medially placed subtle bone reinforcement in the lateral condyle compared with the wild individuals, as well as, slightly higher trabecular bone anisotropy in the medial condyle that is not observed in the wild individuals. This is consistent with the more anisotropic medial femoral condyle compared with the lateral one identified in Sansuke (Richmond et al., 2005).

Within the current knowledge on metabolic differences and trade-offs between cortical and trabecular tissues through life, including during ontogeny, these discrepancies between the clear adaptations at the proximal tibia observed in Sansuke's corticotrabecular complex adjustment (Mazurier et al., 2010) and the less distinct structural changes at the underlying trabecular network are unexpected. Under experimental analyses the human tibial shaft (Erlandson et al., 2012; Weatherholt et al., 2013; Murray and Erlandson, 2022; for other skeletal elements see also Kontulainen et al., 2003; Eser et al., 2009; Erlandson et al., 2012) and mouse tibial shaft (De Souza et al., 2005; Brodt and Silva, 2010) show that cortical bone primarily reflects early life behaviour, while epiphyseal trabecular bone microarchitecture may primarily reflect adult loading. This is consistent with a recent study by Saers et al. (2022) show-

Table 2. Results of Pearson correlation tests between the trabecular bone density (BV/TV), trabecular thickness (Tb.Th.), trabecular spacing (Tb.Sp.), and degree of anisotropy (DA) of the proximal tibia calculated for the left and right tibiae of the bipedally trained macaque Sansuke and for the right tibiae of five wild *Macaca fuscata*.

| Specimens | Parameters | BV/TV | Tb.Th. | Tb.Sp. |
|---|---|---|---|---|
| Sansuke left | Tb.Th. | 0.74* | — | — |
| | Tb.Sp. | **–0.89*** | –0.41* | — |
| | DA | –0.39* | –0.69* | 0.20* |
| Sansuke right | Tb.Th. | **0.81*** | — | — |
| | Tb.Sp. | **–0.92*** | –0.58* | — |
| | DA | –0.52* | **–0.81*** | 0.32* |
| KAS 266 | Tb.Th. | 0.62* | — | — |
| | Tb.Sp. | **–0.86*** | –0.16* | — |
| | DA | –0.30* | –0.48* | –0.02 |
| KAS 269 | Tb.Th. | **0.87*** | — | — |
| | Tb.Sp. | –0.75* | –0.38* | — |
| | DA | 0.22* | 0.47* | 0.10* |
| KAS 276 | Tb.Th. | 0.35* | — | — |
| | TbSp | **–0.88*** | –0.03 | — |
| | DA | –0.12* | 0.22* | –0.04 |
| KAS 281 | Tb.Th. | 0.69* | — | — |
| | Tb.Sp. | **–0.85*** | –0.30* | — |
| | DA | 0.15* | 0.38* | –0.11* |
| KAS 309 | Tb.Th. | 0.79* | — | — |
| | Tb.Sp. | **–0.89*** | –0.54* | — |
| | DA | 0.03 | 0.01 | –0.16* |

Strong correlations ($r > 0.8$) are in bold. *Significant correlations ($P < 0.05$).

ing an adult-like trabecular structure in the calcaneum of 1.5- to 2-year-old Japanese macaques that recently adopted an adult-like locomotion (Saers et al., 2022). Noting that Sansuke started bipedal training at the adult age of 2 years (Nakatsukasa and Hayama, 2003), we would expect that his tibial proximal epiphysis cortical bone thickness would reflect early life wild behaviour, and the trabecular structure would be modelled based on adaptations to bipedal loading. Therefore, in addition to adding information to the discussion about trade-offs between cortical and trabecular tissue throughout life and notably between young and adulthood, our results raise questions about differences in site-specific functional adaptations and notably possible differences between epiphyseal (articular) and diaphyseal cortical adaptations.

In the present case, discrepancies in the functional signal between the subchondral corticotrabecular complex and trabecular tissue of the tibial plateau might reflect differences in sensitivity to the local loading environment during bipedal performances, where the subchondral layers sufficiently withstand and counteract the loads occurring at the knee because of the bipedal training, with no evident impact on the conformation of the deeper trabecular bone. Indeed, in humans it has been demonstrated that the proximal tibia cartilage (including the menisci) and its supporting subchondral bone have corresponding mechanical functions (Lereim et al., 1974; Duncan et al., 1987; Odgaard et al., 1989; Milz and Putz, 1994; McKinley and Bay, 2001; Hoemann et al., 2012) and that the subchondral region exhibits strong architectural response to differences in joint loading regimes (Pontzer et al., 2006; Goliath et al., 2022). In the human patella, another component of the knee joint, a similarly functionally related heterogeneous distribution of the subchondral bone gradually disappears with depth, with most of the deeper trabecular network lacking site-specific structural adaptations (Hoechel et al., 2015). However, although studies have revealed variations of the topographic distribution of the corticotrabecular complex thickness related to differences in locomotor-related loading environment at the knee joint between primates (Ahluwalia, 2000; Mazurier et al., 2010), we still lack enough comparative evidence about the endostructural conformation of this skeletal site in extant primates to reveal any possible link between locomotor mode(s) and site-specific network variation of the trabecular bone beneath the corticotrabecular complex.

Intraspecific variations in lower limb trabecular bone between populations experiencing different level of activities and various loading modalities have been investigated in human populations (Stock, 2006; Ryan and Shaw, 2015; Chirchir et al., 2015, 2017; Saers et al., 2016, 2021; Doershuk et al., 2018; Mulder et al., 2020). First, localized response to loading, rather than systemic variation, is the main driver of these population differences (Chirchir et al., 2017; Doershuk et al., 2018). In addition, all studies showed that on the lower limb, high levels of physical activity contribute to increased bone strength achieved through an increase in bone volume fraction and trabecular thickness. In the case of the present study, while bipedally trained macaques experience an increase in vertical loading at the hip and knee joints during bipedal standing and walking, we did not identify a higher bone volume and trabecular thickness compared to the condition observed in wild individuals. It is therefore important to recall here that the trained macaques spend most of the time running and climbing similar to other wild monkeys (Nakatsukasa et al., 1995; Hirasaki et al., 2004), and thus experience postural/locomotion-related multiaxial loads. In the case of Sansuke, trained from the age of 2 years, a wild behaviour was adopted during childhood. Even though morphological local modifications have been identified in Sansuke's outer and inner skeleton in response to bipedally related constraints (Nakatsukasa et al., 1995; Volpato et al., 2008; Mazurier et al., 2010), the frequency as well as nature of loading locally acting on hip and knee joint in Sansuke during bipedal posture and locomotion against the backdrop of his entire behavioural profile might not have evoked an osseous response.

In conclusion, the high-resolution non-invasive analysis of the postcranial skeleton of a bipedally trained Japanese macaque, Sansuke, continues to provide direct evidence about the rheological and adaptive characteristics of mechanosensitive bony tissues when intermittently facing atypical load related to relatively short but recurrent changes in joint loading environment. In this specific case, the comparative assessment of the functionally related adjustment of the trabecular network at the femoral head

(coxofemoral joint) and the proximal tibia (knee joint) provides new original and partially unexpected results, including on the patterns of network variation characterizing the wild macaque representatives used for comparison. Our results are relevant to attempts to predict and infer locomotory behaviour in fossil primates, including those such as hominins that are defined by the adoption of bipedal locomotion.

## Acknowledgements

Acquisitions of Sansuke's femora and tibiae and of one femur and two tibiae from wild macaques were performed at the ESRF (France) in collaboration with V. Volpato (University of Poitiers) within the EC TNT project led by R. Macchiarelli (University of Poitiers and MNHN, Paris). The remaining specimens were detailed at the Laboratory of Physical Anthropology, Kyoto University, in collaboration with Suo Sarumawashi (Suo Monkey Performance Association) and we are grateful of N. Morimoto (Kyoto University) for taking CT scans of these specimens. For discussion, we thank A. Bardo (MNHN, Paris), C. Dunmore (University of Kent), T. Kivell (University of Kent), Z. Tsegai (University of Kent, Canterbury), and C. Zanolli (PACEA, Bordeaux). Finally, we are grateful to Hiroko Oota, the Associate Editor, and to two anonymous reviewers for constructive comments that considerably improved this manuscript. M.C. was funded by the Fyssen Foundation and the Division of Anthropology of the American Museum of Natural History, New York. This project has received funding from the European Research Council (grant agreement no. 819960).

## References

Ahluwalia K. (2000) Knee Joint Load as Determined by Tibial Subchondral Bone Density: Its Relationship to Gross Morphology and Locomotor Behavior in Catarrhines. PhD thesis, State University of New York, Stony Brook, New York. https://www.proquest.com/openview/9b0b34c5b312299d20adc96fe6c07559/1?pq-origsite=gscholar&cbl=18750&diss=y

Aiello L. and Dean C. (1990) An Introduction to Human Evolutionary Anatomy. Academic Press, New York.

Allen M.R. and Burr D.B. (2014) Bone modeling and remodeling. In: Allen M.R. and Burr D.B. (eds.), Basic and Applied Bone Biology. Academic Press, London, pp. 75–90.

Almécija S., Hammond A.S., Thompson N.E., Pugh K.D., Moyà-Solà S., and Alba D.M. (2021) Fossil apes and human evolution. Science, 372: eabb4363.

Bachmann S., Dunmore C.J., Skinner M.M., Pahr D.H., and Synek A. (2022) A computational framework for canonical holistic morphometric analysis of trabecular bone. Scientific Reports, 12: 5187.

Barak M.M. (2020) Bone modeling or bone remodeling: that is the question. American Journal of Physical Anthropology, 172: 153–155.

Barak M.M., Lieberman D.E., and Hublin J.J. (2011) A Wolff in sheep's clothing: trabecular bone adaptation in response to changes in joint loading orientation. Bone, 49: 1141–1151.

Biewener A.A., Fazzalari N.L., Konieczynski D.D., and Baudinette R.V. (1996) Adaptive changes in trabecular architecture in relation to functional strain patterns and disuse. Bone, 19: 1–8.

Bird E.E., Kivell T.L., and Skinner M.M. (2021) Cortical and trabecular bone structure of the hominoid capitate. Journal of Anatomy, 239: 351–373.

Bird E.E., Kivell T.L., and Skinner M.M. (2022) Patterns of internal bone structure and functional adaptation in the hominoid scaphoid, lunate, and triquetrum. American Journal of Biological Anthropology, 177: 266–285.

Bondioli L., Bayle P., Dean C., Mazurier A., Puymerail L., Ruff C., Macchiarelli R., et al (2010) Morphometric maps of long bone shafts and dental roots for imaging topographic thickness variation. American Journal of Physical Anthropology, 142: 328–334.

Brodt M.D. and Silva M.J. (2010) Aged mice have enhanced endocortical response and normal periosteal response compared with young-adult mice following 1 week of axial tibial compression. Journal of Bone and Mineral Research, 25: 2006–2015.

Burnett J.K. (2017) Bone Strain Change as a Result of a Long Distance Run Modeled on a Finite Element Tibia. PhD dissertation, Iowa State University, Iowa. https://dr.lib.iastate.edu/server/api/core/bitstreams/1cf6226f-021d-4be0-9bc5-0ae0a9ce4c3f/content

Cazenave M., Braga J., Oettlé A., Thackeray J.F., De Beer F., Hoffman J., Endalama E., Redae B.E., Puymerail L., and Macchiarelli R. (2017) Inner structural organization of the distal humerus in *Paranthropus* and *Homo*. Comptes Rendus Palevol, 16: 521–532.

Cazenave M., Braga J., Oettlé A., Pickering T.R., Heaton J.L., Nakatsukasa M., Thackeray F.J., de Beer F., Hoffman J., Dumoncel J., and Macchiarelli R. (2019) Cortical bone distribution in the femoral neck of *Paranthropus robustus*. Journal of Human Evolution, 135: 102666.

Cazenave M., Oettlé A., Pickering T.R., Heaton J.L., Nakatsukasa M., Thackeray J.F., Hoffman J., and Macchiarelli R. (2021) Trabecular organization of the proximal femur in *Paranthropus robustus*: implications for the assessment of its hip joint loading conditions. Journal of Human Evolution, 153: 102964.

Chan Y.H. (2003) Biostatistics 104: correlational analysis. Singapore Medical Journal, 44: 614–619.

Chatani K. (2003) Positional behavior of free-ranging Japanese macaques (*Macaca fuscata*). Primates, 44: 13–23.

Chirchir H., Kivell T.L., Ruff C.B., Hublin J.J., Carlson K.J., Zipfel B., and Richmond B.G. (2015) Recent origin of low trabecular bone density in modern humans. Proceedings of the National Academy of Sciences of the United States of America, 112: 366–371.

Chirchir H., Ruff C.B., Junno J.A., and Potts R. (2017) Low trabecular bone density in recent sedentary modern humans. American Journal of Physical Anthropology, 162: 550–560.

Christen P., Ito K., Ellouz R., Boutroy S., Sornay-Rendu E., Chapurlat R.D., and Van Rietbergen B. (2014) Bone remodelling in humans is load-driven but not lazy. Nature Communications, 5: 1–5.

De Souza R.L., Matsuura M., Eckstein F., Rawlinson S.C.F., Lanyon L.E., and Pitsillides A.A. (2005) Non-invasive axial loading of mouse tibiae increases cortical bone formation and modifies trabecular organization: a new model to study cortical and cancellous compartments in a single loaded element. Bone, 37: 810–818.

Delcamp D.D., Klaaren H.E., and van Meerdervoort H.P. (1988) Traumatic avulsion of the ligamentum teres without dislocation of the hip. Two case reports. Journal of Bone and Joint Surgery, 70: 933–935.

Demange M.K., Kakuda C.M.S., Pereira C.A.M., Sakaki M.H., and Albuquerque R.F.M. (2007) Influence of the femoral head ligament on hip mechanical function. Acta Ortopedica Brasileira, 4: 187–190.

DeMars L.J., Stephens N.B., Saers J.P., Gordon A., Stock J.T., and Ryan T.M. (2021) Using point clouds to investigate the relationship between trabecular bone phenotype and behavior: An example utilizing the human calcaneus. American Journal

of Human Biology, 33: e23468.
Doershuk L.J., Saers J.P.P., Shaw C.N., Jashashvili T., Carlson K.J., Stock J.T., and Ryan T.M. (2018) Complex variation of trabecular bone structure in the proximal humerus and femur of five modern human populations. American Journal of Physical Anthropology, 168: 104–118.
Duncan H., Jundt J., Riddle J.M., Pitchford W., and Christopherson T. (1987) The tibial subchondral plate. A scanning electron microscope study. Journal of Bone and Joint Surgery, 69: 1212–1220.
Dunmore C.J., Wollny G., and Skinner M.M. (2018) MIA-Clustering: a novel method for segmentation of paleontological material. PeerJ, 6: e4374.
Dunmore C.J., Kivell T.L., Bardo A., and Skinner M.M. (2019) Metacarpal trabecular bone varies with distinct hand-positions used in hominid locomotion. Journal of Anatomy, 235: 45–66.
Dunmore C.J., Bardo A., Skinner M.M., and Kivell T.L. (2020a) Trabecular variation in the first metacarpal and manipulation in hominids. American Journal of Physical Anthropology, 171: 219–241.
Dunmore C.J., Skinner M.M., Bardo A., Berger L.R., Hublin J.J., Pahr D.H., and Kivell T.L. (2020b) The position of *Australopithecus sediba* within fossil hominin hand use diversity. Nature Ecology & Evolution, 4: 911–918.
Erlandson M., Kontulainen S., Chilibeck P., Arnold C., Faulkner R., and Baxter-Jones A. (2012) Higher premenarcheal bone mass in elite gymnasts is maintained into young adulthood after long-term retirement from sport: a 14-year follow-up. Journal of Bone and Mineral Research, 27: 104–110.
Eser P., Hill B., Ducher G., and Bass S. (2009) Skeletal benefits after long-term retirement in former elite female gymnasts. Journal of Bone and Mineral Research, 24: 1981–1988.
Fajardo R.J. and Müller R. (2001) Three-dimensional analysis of nonhuman primate trabecular architecture using micro-computed tomography. American Journal of Physical Anthropology, 115: 327–336.
Fajardo R.J., Müller R., Ketcham R.A., and Colbert M. (2007) Nonhuman anthropoid primate femoral neck trabecular architecture and its relationship to locomotor mode. Anatomical Record, 290: 422–436.
Fleagle J.G. (2013) Primate Adaptation and Evolution. Academic Press, New York.
Georgiou L., Kivell T.L., Pahr D.H., and Skinner M.M. (2018) Trabecular bone patterning in the hominoid distal femur. PeerJ, 6: e5156.
Georgiou L., Kivell T.L., Pahr D.H., Buck L.T., and Skinner M.M. (2019) Trabecular architecture of the great ape and human femoral head. Journal of Anatomy, 234: 679–693.
Georgiou L., Dunmore C.J., Bardo A., Buck L.T., Hublin J.J., Pahr D.H., Skinner M.M., et al (2020) Evidence for habitual climbing in a Pleistocene hominin in South Africa. Proceedings of the National Academy of Sciences of the United States of America, 117: 8416–8423.
Goliath J.R., Gosman J.H., Stout S.D., and Ryan T.M. (2022) Ontogenetic patterning of human subchondral bone microarchitecture in the proximal tibia. Biology, 11: 1–22.
Gray A.J. and Villar R.N. (1997) The ligamentum teres of the hip: An arthroscopic classification of its pathology. Arthroscopy, 13: 575–578.
Gross T., Kivell T.L., Skinner M.M., Nguyen N.H., and Pahr D.H. (2014) A CT-image-based framework for the holistic analysis of cortical and trabecular bone morphology. Palaeontologia Electronica, 17: 1–13.
Guanche C.A. (2012) Arthroscopic Anatomy of the Hip. In: Byrd J.W.T. (ed.), Operative Hip Arthroscopy, 3rd ed. Springer-Verlag, New York, pp. 113–120.
Guldberg R.E., Richards M., Caldwell N.J., Kuelske C.L., and Goldstein S.A. (1997) Trabecular bone adaptation to variations in porous-coated implant topology. Journal of Biomechanics, 30: 147–153.
Harrison L.C., Nikander R., Sikiö M., Luukkaala T., Helminen M.T., Ryymin P., Soimakallio S., Eskola H.J., Dastidar P., and Sievänen H. (2011) MRI texture analysis of femoral neck: Detection of exercise load-associated differences in trabecular bone. Journal of Magnetic Resonance Imaging, 34: 1359–1366.
Haxton H.A. (1947) Muscles of the pelvic limb. A study of the differences between bipeds and quadrupeds. Anatomical Record, 98: 337–346.
Hayama S. (1986) Spinal compensatory curvature found in Japanese macaques trained for the aquisition of bipedalism. Journal of Growth, 25: 161–178.
Hayama S., Nakatsukasa M., and Kunimatsu Y. (1992) Monkey performance: the development of bipedalism in trained Japanese monkeys. Acta Anatomica Nipponica, 67: 169–185.
Higurashi Y., Goto R., and Kumakura H. (2018) Intra-individual variation in hand postures during terrestrial locomotion in Japanese macaques (*Macaca fuscata*). Primates, 59: 61–68.
Hirasaki E., Kumakura H., and Matano S. (1993) Kinesiological characteristics of vertical climbing in *Ateles geoffroyi* and *Macaca fuscata*. Folia Primatologica, 61: 148–156.
Hirasaki E., Ogihara N., Hamada Y., Kumakura H., and Nakatsukasa M. (2004) Do highly trained monkeys walk like humans? A kinematic study of bipedal locomotion in bipedally trained Japanese macaques. Journal of Human Evolution, 46: 739–750.
Hirasaki E., Ogihara N., and Nakatsukasa M. (2006) Primates trained for bipedal locomotion as a model for studying the evolution of bipedal locomotion. In: Ishida H., Tuttle R., Pickford M., Ogihara N., and Nakatsukasa M. (eds.), Human Origins and Environmental Backgrounds. Springer, Boston, pp. 149–155.
Hoechel S., Schulz G., and Müller-Gerbl M. (2015) Insight into the 3D-trabecular architecture of the human patella. Annals of Anatomy–Anatomischer Anzeiger, 200: 98–104.
Hoemann C.D., Lafantaisie-Favreau C.H., Lascau-Coman V., Chen G., and Guzman-Morales J. (2012) The cartilage–bone interface. Journal of Knee Surgery, 25: 85–97.
Isler K. (2005) 3D-kinematics of vertical climbing in hominoids. American Journal of Physical Anthropology, 126: 66–81.
Kapandji A.I. (2011) The Physiology of the Joints, Vol. 2: The Lower Limb, 6th edn. Elsevier, Edinburgh.
Kaplan E.B. (1949) The ligamentum teres femoris in relation to the position of the femur. Bulletin of the Hospital for Joint Diseases, 10: 112–117.
Kimura T. (1985) Bipedal and quadrupedal walking of primates: comparative dynamics. In: Kondo S. (ed.), Primate Morphophysiology, Locomotor Analyses and Human Bipedalism. University of Tokyo Press, Tokyo, pp. 81–104.
Kimura T., Okada M., and Ishida H. (1979) Kinesiological characteristics of primate walking: Its significance in human walking. In: Morbeck M.E., Preushoft H., and Comberg N. (eds.), Environment, Behavior, and Morphology: Dynamic Interactions in Primates. Gustav Fischer, New York, pp. 297–311.
Kivell T.L. (2016) A review of trabecular bone functional adaptation: what have we learned from trabecular analyses in extant hominoids and what can we apply to fossils? Journal of Anatomy, 228: 569–594.
Kontulainen S., Sievänen H., Kannus P., Pasanen M., and Vuori I. (2003) Effect of long-term impact-loading on mass, size, and estimated strength of humerus and radius of female racquet-sports players: a peripheral quantitative computed tomography study between young and old starters and controls. Journal of Bone and Mineral Research, 18: 352–359.
Lereim P., Goldie I., and Dahlberg E. (1974) Hardness of the subchondral bone of the tibial condyles in the normal state and in osteoarthritis and rheumatoid arthritis. Acta Orthopaedica, 45: 614–627.
Lovejoy C.O. (2007) The natural history of human gait and pos-

ture: part 3. The knee. Gait & Posture, 25: 325–341.
Macchiarelli R., Nakatsukasa M., Rook L., Viola T.B., and Bondioli L. (2001) Functional adaptation of the iliac and the femoral cancellous network in a bipedal-trained Japanese macaque. American Journal of Physical Anthropology, 114 (S32): 99. https://doi.org/10.1002/ajpa.1036
MacLatchy L. and Müller R. (2002) A comparison of the femoral head and neck trabecular architecture of *Galago* and *Perodicticus* using micro-computed tomography (μCT). Journal of Human Evolution, 43: 89–105.
Mazurier A., Nakatsukasa M., and Macchiarelli R. (2010) The inner structural variation of the primate tibial plateau characterized by high-resolution microtomography. Implications for the reconstruction of fossil locomotor behaviours. Comptes Rendus Palevol, 9: 349–359.
McKinley T.O. and Bay B.K. (2001) Trabecular bone strain changes associated with cartilage defects in the proximal and distal tibia. Journal of Orthopaedic Research, 19: 906–913.
Milz S. and Putz R. (1994) Quantitative morphology of the subchondral plate of the tibial plateau. Journal of Anatomy, 185: 103–110.
Mittra E., Rubin C., and Qin Y.X. (2005) Interrelationship of trabecular mechanical and microstructural properties in sheep trabecular bone. Journal of Biomechanics, 38: 1229–1237.
Mori F., Tachibana A., Takasu C., Nakajima K., and Mori S. (2001) Bipedal locomotion by the normally quadrupedal Japanese monkey, *M. fuscata*: strategies for obstacle clearance and recovery from stumbling. Acta Physiologica et Pharmacologica Bulgarica, 26: 147–150.
Mori S., Nakajima K., Mori F., and Matsuyama K. (2004) Integration of multiple motor segments for the elaboration of locomotion: role of the fastigial nucleus of the cerebellum. Progress in Brain Research, 143: 341–351.
Mori S., Mori F., and Nakajima K. (2006) Higher nervous control of quadrupedal vs bipedal locomotion in non-human primates; common and specific properties. In: Kimura H., Tsuchiya K., Ishiguro A., and Witte H. (eds.), Adaptive Motion of Animals and Machines. Springer, Tokyo, pp. 53–65.
Mulder B., Stock J.T., Saer J.P., Inskip S.A., Cessford C., and Robb J.E. (2020) Intrapopulation variation in lower limb trabecular architecture. American Journal of Physical Anthropology, 173: 112–129.
Murray A.A. and Erlandson M.C. (2022) Tibial cortical and trabecular variables together can pinpoint the timing of impact loading relative to menarche in premenopausal females. American Journal of Human Biology, 34: e23711.
Nakajima K., Mori F., Takasu C., Mori M., Matsuyama K., and Mori S. (2004) Biomechanical constraints in hindlimb joints during the quadrupedal versus bipedal locomotion of *M. fuscata*. Progress in Brain Research, 143: 183–190.
Nakano Y. (1996) Footfall patterns in the early development of the quadrupedal walking of Japanese macaques. Folia Primatologica, 66: 113–125.
Nakano Y., Ishida H., and Hirasaki E. (1996) The change of the locomotor pattern caused by the inclination of the substrata in a Japanese macaque. Primate Research, 12: 79–87.
Nakatsukasa M. (2004) Acquisition of bipedalism: the Miocene hominoid record and modern analogues for bipedal protohominids. Journal of Anatomy, 204: 385–402.
Nakatsukasa M. and Hayama S. (2003) Skeletal response to bipedalism in macaques: with emphasis on cortical bone distribution of the femur. Cour Forschungsinst Senckenberg, 243: 35–45.
Nakatsukasa M., Hayama S., and Preuschoft H. (1995) Postcranial skeleton of a macaque trained for bipedal standing and walking and implications for functional adaptation. Folia Primatologica, 64: 1–29.
Nakatsukasa M., Hirasaki E., and Ogihara N. (2006) Energy expenditure of bipedal walking is higher than that of quadrupedal walking in Japanese macaques. American Journal of Physical Anthropology, 131: 33–37
Negayama K. (1983) Development of locomotor behavior in infant Japanese macaques (*Macaca fuscata*). Annales des Sciences Naturelles: Zoologie, 5: 169–180.
O'Donnell J.M. and Arora M. (2018) A novel and simple classification for ligamentum teres pathology based on joint hypermobility. Journal of Hip Preservation Surgery, 5: 113–118.
O'Donnell J.M., Devitt B.M., and Arora M. (2018) The role of the ligamentum teres in the adult hip: Redundant or relevant? A review. Journal of Hip Preservation Surgery, 5: 15–22.
Odgaard A., Pedersen C.M., Bentzen S.M., Jorgensen J., and Hvid I. (1989) Density changes at the proximal tibia after menisectomy. Journal of Orthopaedic Research, 7: 744–753.
Ogihara N., Usui H., Hirasaki E., Hamada Y., and Nakatsukasa M. (2005) Kinematic analysis of bipedal locomotion of a Japanese macaque that lost its forearms due to congenital malformation. Primates, 46: 11–19.
Ogihara N., Hirasaki E., Kumakura H., and Nakatsukasa M. (2007) Ground-reaction-force profiles of bipedal walking in bipedally trained Japanese monkeys. Journal of Human Evolution, 53: 302–308.
Ogihara N., Makishima H., Aoi S., Sugimoto Y., Tsuchiya K., and Nakatsukasa M. (2009) Development of an anatomically based whole-body musculoskeletal model of the Japanese macaque (*Macaca fuscata*). American Journal of Physical Anthropology, 139: 323–338.
Ogihara N., Makishima H., and Nakatsukasa M. (2010) Three-dimensional musculoskeletal kinematics during bipedal locomotion in the Japanese macaque, reconstructed based on an anatomical model-matching method. Journal of Human Evolution, 58: 252–261.
Ogihara N., Hirasaki E., Andrada E., and Blickhan R. (2018) Bipedal gait versatility in the Japanese macaque (*Macaca fuscata*). Journal of Human Evolution, 125: 2–14.
Okada M. (1985) Primate bipedal walking: comparative kinematics. In: Kondo S (ed.), Primate Morphophysiology, Locomotor Analysis, and Human Bipedalism. University of Tokyo Press, Tokyo, pp. 47–58.
Pahr D.H. and Zysset P.K. (2009) A comparison of enhanced continuum FE with micro FE models of human vertebral bodies. Journal of Biomechanics, 42: 455–462.
Pearson O.M. and Lieberman D.E. (2004) The aging of Wolff's 'law': ontogeny and responses to mechanical loading in cortical bone. Yearbook of Physical Anthropology, 47: 63–99.
Philippon M.J., Rasmussen M.T., Turnbull T.L., Trindade C.A., Hamming M.G., Ellman M.B., and Wijdicks C.A. (2014) Structural properties of the native ligamentum teres. Orthopaedic Journal of Sports Medicine, 2: 2325967114561962.
Polk J.D., Blumenfeld J., and Ahluwalia D. (2008) Knee posture predicted from subchondral apparent density in the distal femur: an experimental validation. Anatomical Record, 291: 293–302.
Pontzer H., Lieberman D.E., Momin E., Devlin M.J., Polk J.D., Hallgrimsson B., and Cooper D.M.L. (2006) Trabecular bone in the bird knee responds with high sensitivity to changes in load orientation. Journal of Experimental Biology, 209: 57–65.
Preuschoft H., Hayama S., and Günther M.M. (1988) Curvature of the lumbar spine as a consequence of mechanical necessities in Japanese macaques trained for bipedalism. Folia Primatologica, 50: 42–58.
Profico A., Bondioli L., Raia P., O'Higgins P., and Marchi D. (2021) Morphomap: an R package for long bone landmarking, cortical thickness, and cross-sectional geometry mapping. American Journal of Physical Anthropology, 174: 129–139.
Puymerail L. (2013) The functionally-related signatures characterizing the endostructural organisation of the femoral shaft in modern humans and chimpanzee. Comptes Rendus Palevol, 12: 223–231.
R Core Team (2018) R: A Language and Environment for Statistical Computing. R Foundation for Statistical Computing, Vienna.

http://www.R-project.org/.
Raichlen D.A., Gordon A.D., Foster A.D., Webber J.T., Sukhdeo S.M., Scott R.S., Gosman J.H., and Ryan T.M. (2015) An ontogenetic framework linking locomotion and trabecular bone architecture with applications for reconstructing hominin life history. Journal of Human Evolution, 81: 1–12.
Rao J., Zhou Y.X., and Villar R.N. (2001) Injury to the ligamentum teres: mechanism, findings, and results of treatment. Clinics in Sports Medicine, 20: 791–800.
Renault J.B., Carmona M., Tzioupis C., Ollivier M., Argenson J.N., Parratte S., and Chabrand P. (2020) Tibial subchondral trabecular bone micromechanical and microarchitectural properties are affected by alignment and osteoarthritis stage. Scientific Reports, 10: 1–10.
Richmond B.G., Nakatsukasa M., Griffin N.L., Ogihara N., and Ketcham R.A. (2005) Trabecular bone structure in a bipedally-trained macaque. American Journal of Physical Anthropology, 126 (S40): 175–176. https://doi.org/10.1002/ajpa.20217
Ritter M.A., Davis K.E., Small S.R., Merchun J.G., and Farris A. (2014) Trabecular bone density of the proximal tibia as it relates to failure of a total knee replacement. Bone & Joint Journal, 96: 1503–1509.
Roberts B.C., Solomon L.B., Mercer G., Reynolds K.J., Thewlis D., and Perilli E. (2017) Joint loading and proximal tibia subchondral trabecular bone microarchitecture differ with walking gait patterns in end-stage knee osteoarthritis. Osteoarthritis and Cartilage, 25: 1623–1632.
Robling A.G., Hinant F.M., Burr D.B., and Turner C.H. (2002) Improved bone structure and strength after long-term mechanical loading is greatest if loading is separated into short bouts. Journal of Bone and Mineral Research, 17: 1545–1554.
Ruff C.B., Holt B., and Trinkaus E. (2006) Who's afraid of the big bad Wolff? 'Wolff's law' and bone functional adaptation. American Journal of Physical Anthropology, 129: 484–498.
Ryan T.M. and Ketcham R.A. (2002a) The three-dimensional structure of trabecular bone in the femoral head of strepsirrhine primates. Journal of Human Evolution, 43: 1–26.
Ryan T.M. and Ketcham R.A. (2002b) Femoral head trabecular bone structure in two omomyid primates. Journal of Human Evolution, 43: 241–263.
Ryan T.M. and Ketcham R.A. (2005) Angular orientation of trabecular bone in the femoral head and its relationship to hip joint loads in leaping primates. Journal of Morphology, 265: 249–263.
Ryan T.M. and Krovitz G.E. (2006) Trabecular bone ontogeny in the human proximal femur. Journal of Human Evolution, 51: 591–602.
Ryan T.M. and Shaw C.N. (2012) Unique suites of trabecular bone features characterize locomotor behavior in human and non-human anthropoid primates. PLoS One, 7: 1–11.
Ryan T.M. and Shaw C.N. (2015) Gracility of the modern *Homo sapiens* skeleton is the result of decreased biomechanical loading. Proceedings of the National Academy of Sciences of the United States of America, 112: 372–377.
Ryan T.M. and Walker A. (2010) Trabecular bone structure in the humeral and femoral heads of anthropoid primates. Anatomical Record, 293: 719–729.
Ryan T.M., Carlson K.J., Gordon A.D., Jablonski N., Shaw C.N., and Stock J.T. (2018) Human-like hip joint loading in *Australopithecus africanus* and *Paranthropus robustus*. Journal of Human Evolution, 121: 12–24.
Saers J.P.P., Cazorla-Bak Y., Shaw C.N., Stock J.T., and Ryan T.M. (2016) Trabecular bone structural variation throughout the human lower limb. Journal of Human Evolution, 97: 97–108.
Saers J.P.P., DeMars L.J., Stephens N.B., Jashashvili T., Carlson K.J., Gordon A.D., Shaw C.N., Ryan T.M., and Stock J.T. (2021) Combinations of trabecular and cortical bone properties distinguish various loading modalities between athletes and controls. American Journal of Physical Anthropology, 174: 434–450.
Saers J.P., Gordon A.D., Ryan T.M., and Stock J.T. (2022) Growth and development of trabecular structure in the calcaneus of Japanese macaques (*Macaca fuscata*) reflects locomotor behavior, life history, and neuromuscular development. Journal of Anatomy, 241: 67–81.
Saparin P., Scherf H., Hublin J.-J., Fratzl P., and Weinkamer R. (2011) Structural adaptation of trabecular bone revealed by position resolved analysis of proximal femora of different primates. Anatomical Record, 294: 55–67.
Shaw C.N. and Ryan T.M. (2012) Does skeletal anatomy reflect adaptation to locomotor patterns? Cortical and trabecular architecture in human and nonhuman anthropoids. American Journal of Physical Anthropology, 147: 187–200.
Skerry T. (2000) Biomechanical influences on skeletal growth and development. In: O'Higgins P. and Cohn M.J. (eds.), Development, Growth and Evolution. Implications for the Study of the Hominoid Skeleton. Linnean Society of London, San Diego and London, pp. 29–39.
Stock J.T. (2006) Hunter-gatherer postcranial robusticity relative to patterns of mobility, climatic adaptation, and selection for tissue economy. American Journal of Physical Anthropology, 131: 194–204.
Su A. and Carlson K.J. (2017) Comparative analysis of trabecular bone structure and orientation in South African hominin tali. Journal of Human Evolution, 106: 1–18.
Sukhdeo S., Parsons J., Niu X.M., and Ryan T.M. (2020) Trabecular bone structure in the distal femur of humans, apes, and baboons. Anatomical Record, 303: 129–149.
Sylvester A.D. and Terhune C.E. (2017) Trabecular mapping: leveraging geometric morphometrics for analyses of trabecular structure. American Journal of Physical Anthropology, 163: 553–569.
Synek A., Dunmore C.J., Kivell T L., Skinner M.M. and Pahr D.H. (2019) Inverse remodelling algorithm identifies habitual manual activities of primates based on metacarpal bone architecture. Biomechanics and Modeling in Mechanobiology, 18: 399–410.
Tardieu C. (1983) L'articulation du genou: analyse morphofonctionnelle chez les primates et les hominidés fossiles. FeniXX. Éditions du Centre national de la recherche scientifique, Paris.
Tsegai Z.J., Kivell T.L., Gross T., Nguyen N.H., Pahr D.H., Smaers J.B., and Skinner M.M. (2013) Trabecular bone structure correlates with hand posture and use in hominoids. PLoS One, 8: e78781.
Tsegai Z.J., Skinner M.M., Pahr D.H., Hublin J.J., and Kivell T.L. (2018) Systemic patterns of trabecular bone across the human and chimpanzee skeleton. Journal of Anatomy, 232: 641–656.
van Arkel R.J., Amis A.A., Cobb J.P., and Jeffers J.R.T. (2015) The capsular ligaments provide more hip rotational restraint than the acetabular labrum and the ligamentum teres: an experimental study. Bone & Joint Journal, 97: 484–491.
Veneziano A., Cazenave M., Alfieri F., Panetta D., and Marchi D. (2021) Novel strategies for the characterization of cancellous bone morphology: virtual isolation and analysis. American Journal of Physical Anthropology, 175: 920–930.
Volpato V., Viola T.B., Nakatsukasa M., Bondioli L., and Macchiarelli R. (2008) Textural characteristics of the iliac-femoral trabecular pattern in a bipedally trained Japanese macaque. Primates, 49: 16–25.
Weatherholt A.M., Fuchs R.K., and Warden S.J. (2013) Cortical and trabecular bone adaptation to incremental load magnitudes using the mouse tibial axial compression loading model. Bone, 52: 372–379.
Wickham H. (2009) ggplot2: Elegant Graphics for Data Analysis. Springer, New York.